Design of a Multi-Function Doppler Processing Platform

1st Jerker Taudien
Teledyne RD Instruments
Poway, CA
jerker.taudien@teledyne.com

2nd Paul Devine
Teledyne RD Instruments
Poway, CA
paul.devine@teledyne.com

3rd William Meachum
Teledyne RD Instruments
Poway, CA
william.meachum@teledyne.com

4th Ian Cassimatis
Teledyne RD Instruments
Poway, CA
ian.cassimatis@teledyne.com

5th Loic Michel
Teledyne RD Instruments
La Gaude, France
loic.michel@teledyne.com

***Abstract*—Acoustic Doppler current profilers (ADCPs) measure the relative velocity between the instrument and a group of scatterers in the water column by transmitting acoustic pulses along multiple beams that point in different directions and measure the Doppler shift of the acoustic signal that is scattered back towards the instrument in each beam. There exists a large and diverse set of applications for ADCPs—each of the applications can benefit from different instrument configurations and tradeoffs; this tradespace can, at a high level, be partitioned into the following variables: size, power, range, variance, resolution, accuracy, and features. A new Doppler-sonar platform called Proteus has been developed, with the objective to expand the existing ADCP tradespace. Several new improvements and features have been introduced in this platform, including reduced size, reduced power consumption, configurable transmit power, frequency agility, linear IQ data, and an integrated attitude and heading reference system (AHRS), to name a few. A new Workhorse Proteus line of ADCPs, built on the Proteus platform, inherit the data-quality, reliability, and many other aspects of the trusted legacy Workhorse while leveraging the latest in technology. Test results are presented in this work, demonstrating the improvements and new features of the 300 kHz Workhorse Proteus ADCP.**

***Index Terms*—acoustic Doppler current profiler, ADCP, currents, sonar platform, AHRS, edge processing,**

I. Introduction

Doppler sonars, including acoustic Doppler current profilers (ADCPs) and Doppler velocity logs (DVLs) measure the relative velocity between the instrument and a group of scatterers by transmitting acoustic pulses along multiple beams that point in different directions and measure the Doppler shift of the acoustic signal that is scattered back towards the instrument in each beam. The group of scatterers can consist of either suspended particles in the water column to measure currents or a boundary surface, for example the ocean floor, to measure velocity over ground. The former case is referred to as water profiling and the latter case is referred to as bottom track. A common configuration consists of four beams separated in azimuth by 90° and elevated from vertical by a common angle referred to as the Janus angle, α_J. Other configurations exist, for example a three-beam configuration, but this work focuses on the Janus configuration. The projection of the relative velocity between the instrument and the scatterers onto a unit vector, parallel to the beams, yields the radial velocity

$$v_{ri} = \boldsymbol{v} \cdot \boldsymbol{e}_i, \tag{1}$$

where $\boldsymbol{v}$ is the relative velocity and $\boldsymbol{e}_i$ is the unit vector parallel to beam i.

A three-dimensional velocity vector can then be obtained by transforming the radial beam velocities to an orthogonal coordinate system aligned to a particular reference frame; two commonly-used reference frames are the instrument and earth reference frames.

There exists a large number of applications for Doppler sonars —the applications can be divided into water profiling and bottom track. The following are some common water-profiling applications:

- current measurements at multiple depths in the water column allowing measurements of ocean transport and circulation,
- wave height, period, and direction measurements as well as water level changes for use in coastal or offshore engineering projects,
- volumetric discharge meaurements in river estuaries and channels for use in flood forecasting and water resources management,
- acoustic backscatter measurements to calibrate for a site-specific concentration of suspended sediment concentration and total sediment load,
- ADCP deployment under ice to measure ice movement and thickness to understand climate change in polar regions, and
- assessment of volumetric transport and mixing to assist in the fate of marine contaminants and pollution and assess the health of aquatic environments.

The following are some commmon bottom-track applications:

- vessel velocity removal from vessel-mounted current-profiling surveys,

- vehicle navigation providing accurate measurements of speed over ground and altitude above the bottom for improved vehicle control,
- velocity over ground for vehicle station-keeping applications, and
- velocity over ground to aid inertial-navigation systems (INS) to reduce position drift over time.

Each of the applications can benefit from different instrument configurations and tradeoffs; this tradespace can, at a high level, be partitioned into the following variables: size, power, range, variance, resolution, accuracy, and features.

The first application of Doppler backscatter for current-measurements was explored by Koczy et al. in the 1960s, utilizing a single-beam, narrowband, 10 MHz bistatic current meter [1]. The first ADCP, capable of a three-dimensional velocity measurement, was developed by Wiseman et al. in 1972 and was used for turbulence studies in estuaries [2]. One of the first commercially successful ADCPs was the DCP-4400, developed by Rowe and Young in the late 1970s and it was able to profile to over 100 m [3] [4] [5]. These instruments all used narrowband signaling—one shortcoming of the narrowband ADCP is the resolution-range-variance tradeoff, discussed in more detail in Section II. Brumley et al. addressed this shortcoming when they invented the broadband ADCP in 1991 [6]. Broadband signaling significantly increases the time-bandwidth product, resulting in multiple independent velocity samples per ping and a reduced velocity-error variance for a given pulse length. The improved broadband performance can be traded off between reduced velocity variance, reduced averaging time, or increased spatial resolution.

In 1995 the first ADCP with a phased-array transducer was built and results were reported by Yu and Gordon [7]. Their invention operated at 38 kHz and significantly reduced the transducer size by forming four Janus beams at 30° Janus angle from a single transducer aperture. Phased-array transducers have a size advantage over piston transducers—this advantage is especially significant for low-frequency systems that would be prohibitively large if piston transducers were utilized. For ADCP applications there are two drawbacks of the phased-array transducer with 30° Janus angle, namely the narrower relative bandwidth and increase side-lobe exclusion zone, when compared to 20° Janus angle piston transducers. This side-lobe exclusion drawback was eliminated in 2019 when the 44 kHz Pinnacle ADCP with a 20° Janus angle phased-array transducer was invented [8] [9].

There have been significant advancements in system integration, size optimization through component miniaturization, power optimization, ping rate optimization, and addition of new features in Doppler sonars. One of the earliest, and most commercially successful, systems leveraging broadband signaling was the Teledyne RDI Workhorse ADCP, launched in 1995 [10]. Other significant advancements in system integration includes the AD2CP platform development by Nortek that was first included in the long-range Signature-75 ADCP [11].

Cell-mapping is an algorithms that uses measured attitude to correct the vertical position of ADCP cells. The original RDI NarrowBand ADCP (1983), BroadBand ADCP (1990), and Workhorse ADCP (1995) included this algorithm, but used tilt sensing that is susceptible to disturbances from accelerations due to wave motion. Attitude and heading reference systems (AHRS) improve tilt sensing by the use of gyros to reduce the sensitivity to acceleration-induced attitude errors; in recent years AHRS sensors have been integrated into ADCPs [12] [13].

A new Doppler-sonar platform named Proteus, after the adaptable Greek sea god, has been developed at Teledyne RDI. Like its namesake, Proteus is a flexible platform that provides the ability to change its functionality in response to changing ocean or estuary monitoring applications. Over 40 years of experience in the design of Doppler-sonar products has been leveraged during the development of the Proteus platform. This platform inherits the data-quality and reliability of the legacy Workhorse, leverages the latest in technology, and provides many new features. The first product that is built on the Proteus platform is the Workhorse Proteus ADCP, which has the potential to enable new applications, improves the performance of existing applications, and expands the ADCP tradespace.

The remainder of this paper is divided into five sections: tradespace optimization, Proteus platform, Workhorse Proteus, test results, and conclusion. Tradespace optimization is discussed II, followed by design and features of the Proteus platform and Workhorse Proteus ADCP in Section III and IV, respectively. Test results are discussed in Section V and in Section VI we discuss additional work, and testing that would be applicable to the Proteus platform and Workhorse Proteus ADCP.

II. Tradespace Optimization

The ADCP tradespace can, at a high level, be partitioned into the following variables: size, power, range, variance, resolution, accuracy, and features. There is a relationship between these variables and any one or a group of variables can be optimized at the expense of the other variables. For example, increased aperture size improves range, variance, and long-term accuracy [14] [15]. The definition of long-term accuracy is the residual accuracy after averaging a large number of pings, such that the contribution from velocity-error variance approaches zero. Power can be divided into three components: sleep power, active power, and transmit power. Sleep and active power solely depend on the electronics and firmware architecture and both affect the deployment duration. Transmit power, on the other hand, affects maximum range, and for low signal-to-noise ratio (SNR) also affects variance [16]. Doppler sonars are peak-power limited due to cavitation and shock loss [17]. Therefore, the maximum range does not increase with increased transmit power beyond the intensity at which cavitation and shock occur.

Signal bandwidth controls the tradeoff between variance and range; higher bandwidth favors decreased variance at the expense of reduced range. Another important control

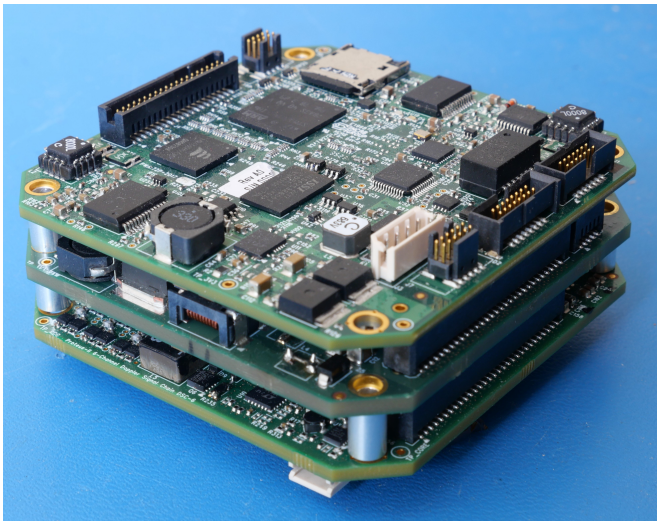

Fig. 1: Proteus board stack

parameter is the water-profiling cell size; it controls the resolution–range–variance tradeoff [6]. High resolution is achieved by transmitting short pulses, but both range and velocity variance suffer. Alternatively, a long pulse provides longer range and lower velocity variance than a short pulse, but the spatial resolution is reduced. Further, velocity variance can be reduced by temporal averaging, but the tradeoff is reduced temporal resolution.

Each of the many Doppler-sonar applications can benefit from different instrument configurations and tradeoffs. The objective of the Proteus platform and the Workhorse Proteus ADCP is to expand the tradespace and provide maximum flexibility in configurability to best tailor the setup to the particular applications of interest. These advancements were accomplished by leveraging state-of-the-art electronics, utilizing several highly-capable microcontroller units (MCUs), and tight integration of new features.

III. Proteus Platform

A new Doppler-sonar platform called Proteus, after the adaptable Greek sea god, has been developed. The objective was to expand the tradespace, provide maximum configuration flexibility, integrate new features, and provide the highest possible reliability and integrity of Doppler data.

The size of the platform has been reduced significantly with the internal electronics measuring 76x76 mm; a picture of the Proteus stack is shown in Fig. 1.

The Proteus sleep power has been reduced by 40% to about 400 μW compared to the Workhorse platform, which was achieved by using non-volatile memories instead of persistent static RAM. Further the average active power has been reduced from about 1.8 W of Workhorse to 1.6 W. A new transmit circuit features configurable transmit power to enable either long range, long deployment duration, or a combination thereof. Higher transmit power allows longer range when ADCP users require high resolution measurements but do not want to sacrifice as much range as they would have in a previous generation Workhorse ADCP. Proteus also provides a boost converter that ensures that the transmit power is constant throughout the deployment, even when the battery voltage droops towards the end of a deployment, providing more consistent profiling ranges over the life of the battery and more consistent water column echo intensity for sediment dynamics and biological oceanographic applications.

The Proteus platform is frequency agile and supports frequencies from 10 kHz up to 5 MHz. There are six channels present allowing for four Janus beams and a vertical beam with one channel to spare for future applications. The receiver is fully linear with 24-bit IQ resolution, improving the SNR performance of the RSSI data and bottom-track detection along with very precise RSSI amplitude information. A real-time clock (RTC) with 2 ppm accuracy is included for time stamping—this accuracy is equivalent to a maximum drift of 63 s in one year.

The platform includes an integrated gyro-stabilized AHRS for very accurate heading, pitch, and roll measurements along with AHRS-aided cell mapping, providing high-quality geo-referenced ADCP cells in dynamic environments. The integrated sensor module consists of a 3-axis accelerometer, 3-axis magnetometer, and 3-axis gyroscope. The sensor measurements are combined into an AHRS solution using an Extended Kalman filter with the quaternion $\boldsymbol{q} = [q_w \; q_x \; q_y \; q_z]^T$ as the state vector. The high-quality inertial sensors are meticulously calibrated in the factory to provide the best possible performance. The system also supports compass field calibration to minimize errors from hard and soft iron disturbances. The static accuracy of the AHRS system has been tested on a calibration fixture in Poway, CA and the root-mean square (RMS) accuracy achieved was 0.3° heading, and 0.1° pitch and roll.

Doppler processing is performed on a dedicated MCU and a separate MCU called Catalyst is used for post processing along with user I/O. This partitioning allows for optimization for efficient processing and ping rates in excess of 16 Hz and a rich set of I/O including RS232, RS422, and Ethernet. The high ping rate along with configurable averaging can be traded off between decreased variance or improved temporal or spatial resolution.

Edge processing is implemented on the Catalyst MCU, which can transform raw measurements into other coordinate frames such as the earth frame. The edge processing provides both flexibility to process several different workflows and preserves the raw data for processing after the completion of a deployment. This onboard processing further expands the use of the ADCP in real-time applications on autonomous survey platforms or in ocean-observing systems that use low bandwidth telemetry systems. Future onboard real-time calculations could include the removal of vessel speed over ground, advanced data quality assurance estimates, statistical analysis such as current rose, maximum wave height from zero up-crossing analysis, directional wave spectrum, dissipation estimates such as Reynolds stresses and turbulence, and de-

Fig. 2: Workhorse Proteus monitor ADCPs. From left to right: 300 kHz, 600 kHz, and 1200 kHz

tiding of current data.

IV. Workhorse Proteus

The Workhorse line of ADCPs and DVLs is one of the most ubiquitous Doppler-sonar product lines—over 13,000 units have been deployed to date. The new Workhorse Proteus line of ADCPs, built on the Proteus platform, inherit the data-quality, reliability, and many other aspects of the trusted legacy Workhorse. It also leverages the latest in technology, and provides several new features.

A. Similarities

Workhorse Proteus ADCPs are offered in the familiar 300 kHz, 600 kHz, and 1200 kHz acoustic frequencies with 20° Janus angle, which is identical to the legacy Workhorse—a picture of the monitor version of the Workhorse Proteus family is shown in Fig. 2. The wide range of acoustic frequencies ensures that that optimal tradeoff between range and resolution can be found for most coastal applications. The 20° beam angle ensures that the instrument can profile very close to boundaries just like the legacy Workhorse.

The standard and most robust water-profiling mode used in Workhorse Proteus is called water-mode 2 (WM2). It is similar to the legacy WM1, but uses linear instead of 1-bit IQ data for velocity processing. The standard bottom-track mode in Workhorse Proteus is also very similar to the legacy Workhorse bottom-track mode. The same robustness and reliability of the legacy Workhorse can be expected from the Workhorse Proteus water-profiling and bottom-track modes.

B. Improvements

Several new improvements are available in the Workhorse Proteus line of ADCPs. The instrument sizes are significantly reduced compared to the legacy Workhorse. Specifically, the 1200 kHz instrument diameter is reduced from 203 mm to 121 mm and the height is reduced from 216 mm to 154 mm. The 300 kHz and 600 kHz instruments are offered in sentinel and monitor versions, but the 1200 kHz instrument is only offered in a monitor version at the moment; the small form factor makes it impractical to outfit the 1200 kHz instrument with an alkaline battery pack. Lithium battery packs may be offered in the future for all three frequencies. The depth rating of the Workhorse Proteus line of products has increased from 200 m to 300 m.

The maximum recorder capacity has increased from 4 GB to 64 GB. The Workhorse Proteus utilizes a SafeFAT file system on the SD-card recorder, with built in protection against data loss during power outage, for maximum reliability. The input voltage is expanded from 20–50 V to 10.7—50 V.

The linear receiver of the Proteus platform and digital signal-processing chain, implemented in a field-programmable gate array (FPGA), provides for precision measurements of the signal level in each cell. The in-phase and quadrature (IQ) data generated by the FPGA is used for velocity measurements along with digital received signal strength indicator (RSSI) data generation. The legacy Workhorse processed velocity from 1-bit IQ data and used an analog integrated circuit (IC) to measure RSSI amplitude. Digital RSSI is advantageous due to the near-perfect relative amplitude measurements obtained from

$$\text{RSSI} = \text{round}\left(\frac{255}{12.75}\log 10(I^2+Q^2) - 27.9682\right). \quad (2)$$

The offset and scaling constants are selected such that the maximum possible IQ values map to RSSI = 255 and the slope is exactly 0.5 dB/count.

The four Janus beams of the legacy Workhorse are augmented with a vertical beam in Workhorse Proteus, as shown in Fig. 2. There are two vertical-beam processing modes: vertical-beam profiling and vertical-beam ranging. The vertical-beam profiling mode is similar to the standard WM2 of the Janus beams and supports the same cell sizes. The vertical-beam ranging mode provides high-resolution range estimates to boundary surfaces such as the bottom, surfaces, ice sheets, etc. Data from the vertical beam is presented in Section V-C. The ranging ping uses a range-optimized transmit pulse and high resolution receive sampling that is focused on identifying the range to a boundary with higher resolution than possible with a ping optimized for current profiling. This ping type will provide improved bathymetry measurements from the vertical beam when used from a survey vessel or improved accuracy of acoustic surface track based wave-height measurement when used from a sub-surface mooring.

Efficient processing on the Proteus platform has increased the ping rate of the high-frequency 1200 kHz to 16 Hz. This high ping rate along with configurable averaging can be

traded off between decreased variance or improved temporal or spatial resolution. Additionally, all improvements mentioned in the Proteus Platform Section III are included in the Workhorse Proteus.

V. Test Results

Testing took place from July 25 through August 29, 2024, in the Mediterranean Sea outside of Nice in France. A legacy 300 kHz Workhorse and a 300 kHz Workhorse Proteus ADCP were tested, mounted to a vessel.

The water temperature at the test location was quite warm with a surface temperature of 29°C. Data from the World Ocean Atlas was used to estimate the temperature profile; the average temperature throughout the top 100 m was estimated to be 18°C. This temperature, along with 35 ppt salinity were used for performance predictions. The average absorption coefficient, α, was calculated to be 0.096 dB/m and the nominal volume-scattering coefficient used for the performance predictions was $S_v = -80$ dB.

A. Water Profiling

A vessel-mounted survey with the Workhorse Proteus ADCP was conducted outside of Antibes, France. The transect consisted of traveling in a straight track at 2.5 m/s towards shore, turning around, and traveling back in the same track, as shown in Fig. 3. This maneuver is advantageous to be able to check the consistency of the ADCP data. After removing vessel motion, using bottom-track data, and transforming the measured ADCP velocity profile to earth coordinates, the away and back tracks should measure the same velocity profile, but mirrored around the turn-around location. The east and north velocity components, using 2 m cell size, of the velocity profiles are shown in Fig. 4.

The Workhorse Proteus bottom-tracking ping was able to accurately remove the speed over ground and resolve the very low 15 cm/s magnitude currents and characterize a rotational flow from a near surface eddy. The measured velocities near the surface (6.77 meters depth) were less than 5 cm/sec directed to the north west at the western inshore extent of the survey, increasing in speed and rotating about 90° flowing to the south west at the eastern offshore extent of the survey. We observed a significant shear in the water column with the currents at the deeper depths predominantly flowing to the north in the near-shore region and to the north west in the offshore region. Current speed was minimum in the mid water column, increasing in speed as depth increased from 22 m to 38 m. The contour plot of the north and east components of velocity show an abrupt vertical shear at a depth of 18 m. There was also a very distinct sub-surface jet in the north east direction extending from 18 m to 35 m depth.

B. Bottom Track

A standard bottom-track range test was performed with Workhorse Proteus, starting in a shallow location and gradually traveling to a deeper location until bottom lock was lost. The detected range, for the four Janus beams, is shown in

Fig. 3: Vessel mounted ADCP survey track plotted on map of coast by Antibes, France

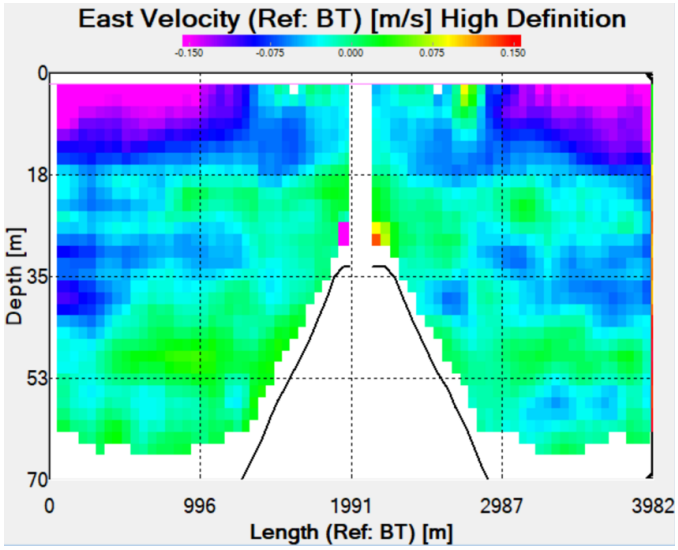

(a) East Velocity

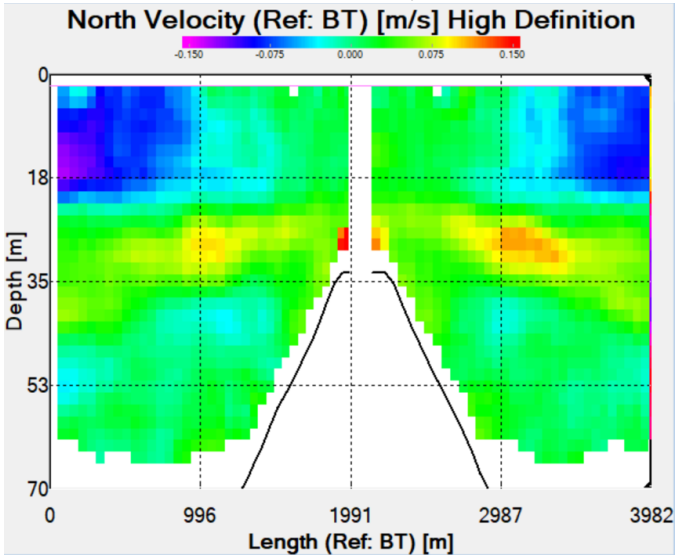

(b) North Velocity

Fig. 4: Vessel-mounted survey with WHP ADCP out and back

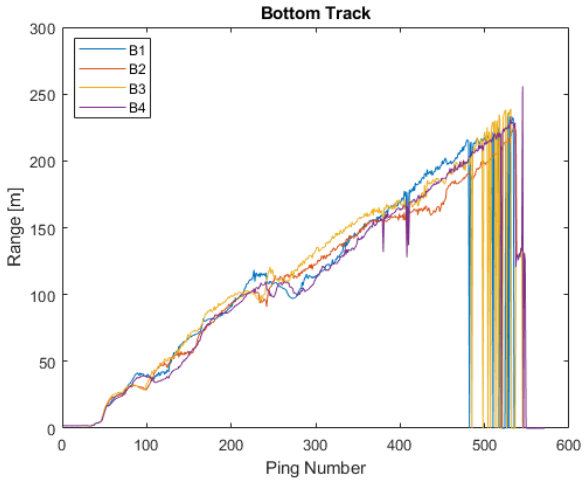

Fig. 5: Bottom track range test

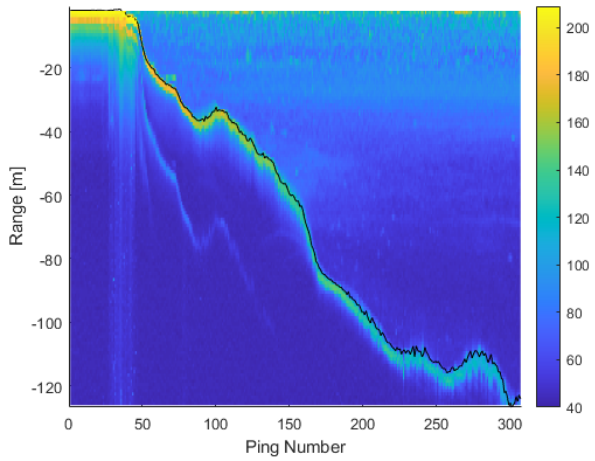

Fig. 6: Vertical-profiling ping RSSI amplitude and overlaid vertical-ranging ping altitude measurement

Fig. 5. The mean range, at which consistent bottom detection occurred, was 198 m. The predicted range, assuming a mean water temperature of 15 °C, was 201 m. Missed bottom detection is indicated by the range being set to 0.

C. Vertical Beam

The vertical-beam profiling and vertical-beam ranging pings were configured as interleaved during a survey from shallow to deep, starting at about 2 m depth and ending at over 250 m depth. The cell size was configured to 1 m and there were a total of 125 cells. Maximum achieved profiling range was about 60 m on average, using a correlation coefficient of 0.5 as the threshold. The ranging ping was able to bottom track to 275 m of altitude. In Fig. 6, the RSSI amplitude is plotted over time along with an overlaid range-ping estimate of the altitude. It can be seen that the range-ping estimate of altitude closely matches the echo intensity corresponding to the bottom. It should be noted that the amplitude at ranges greater than the bottom are not valid and should be ignored.

D. Variable Power Mode

The configurable power transmit circuit on the Proteus platform was discussed in Section III. The tests in this section focus on the relationship between transmit power and range along with the resolution–range–variance tradeoff. Range depends on the absorption coefficient α and volume scattering coefficient S_v, as discussed in Section V. We attempted to perform all testing in the same geographical location, but found that the volume-scattering profile $S_v(h)$, where h is altitude, varied quite a bit from test to test, due to boat drift. Therefore, the measured maximum water-profiling range for the different configurations contain variation due the variation of $S_v(h)$. The predicted and measured maximum water-profiling ranges are presented in Table I.

The maximum range is taken as the range at which the correlation is 64 counts, corresponding to a correlation coefficient $\rho = 0.5$ and SNR = 0 dB. It can be seen that the maximum

TABLE I: Predicted and measured water-profiling range.

ADCP	Bandwidth %	Cell Size m	Power W	Range Predicted m	Range Measured m
WH	25	4	25	83	66
	6.25	8	25	120	92
WHP	25	4	18	79	69
			25	83	73
			73	94	77
			129	99	87
	6.25	8	18	115	85
			25	120	97
			73	132	113
			129	137	137

range increases with reduced bandwidth, increased cell size, and increased transmit power, as expected. However, there are significant errors between the predicted and measured range for several of the configurations. This error is likely due to variation of the volume-scattering profile $S_v(h)$. The averaged correlation profiles for the different transmit power levels are shown in Fig. 7. It is apparent that there are shape differences in the profiles, which are likely due to spatially-varying $S_v(h)$ profiles. However, it has been demonstrated that on average the maximum water-profiling range increases with increasing transmit power level.

E. AHRS

Legacy ADCPs, including the Workhorse, use a tilt-compensated compass which comprises 3-axes accelerometers and magnetometers to provide estimated heading, pitch, and roll. This works well when conditions are relatively static; however, when dynamic motion is present, non-gravity acceleration affects the tilt measurement, which leads to degraded tilt and heading accuracy.

The Workhorse Proteus integrated gyro-stabilized AHRS was compared with NMEA-0183 heading from a Hemisphere

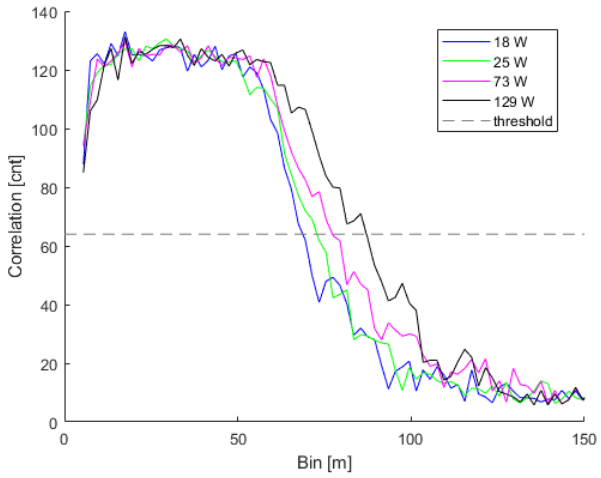

(a) Bandwidth = 25% and cell size = 4 m

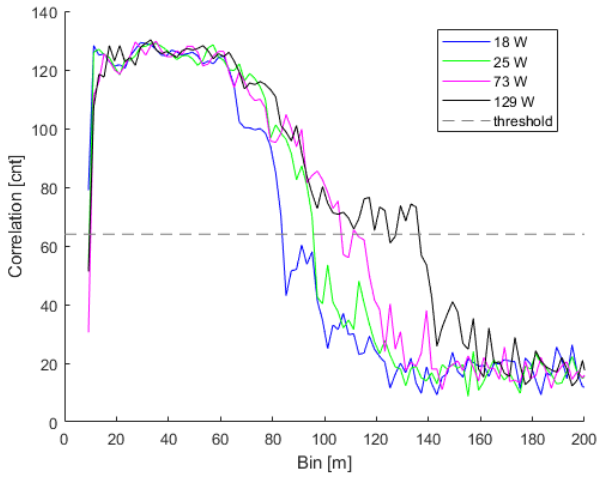

(b) Bandwidth = 6.25% and cell size = 8 m

Fig. 7: Workhorse Proteus correlation profiles for different bandwidths, cell sizes, and transmit power levels

V102 Vector GPS while the vessel made three complete circles, shown in Fig. 8. Once corrected for local magnetic declination, the heading from the Proteus AHRS demonstrated an RMS error of 0.98 degrees with respect to the GPS heading.

The magnetic field and acceleration sampled from the Workhorse Proteus internal sensors at 104 Hz was post processed as a non-gyro stabilized tilt-compensated compass, using the e-compass algorithm

$$\boldsymbol{R} = [\boldsymbol{m} \times \boldsymbol{a}, \boldsymbol{a} \times (\boldsymbol{m} \times \boldsymbol{a}), \boldsymbol{a}], \tag{3}$$

where $\boldsymbol{R}$ is the rotation matrix, $\boldsymbol{a}$ is the acceleration vector, and $\boldsymbol{m}$, is the magnetometer vector. The Workhorse Proteus AHRS attitude was compared with the e-compass attitude for a dynamic data set, shown in Fig. 9. It is very clear that the attitude estimated from the e-compass algorithm is much noisier than that of the AHRS.

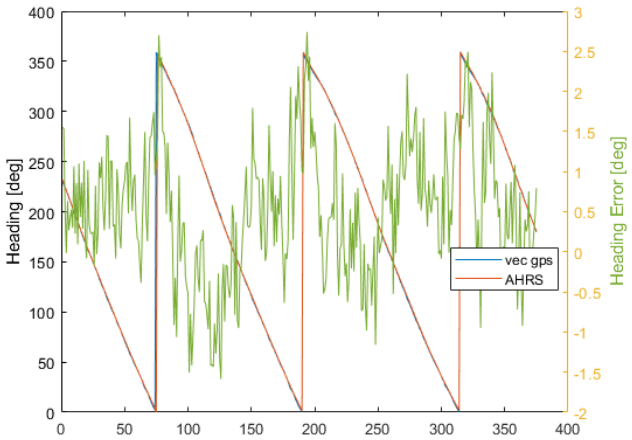

Fig. 8: AHRS heading comparison with GPS

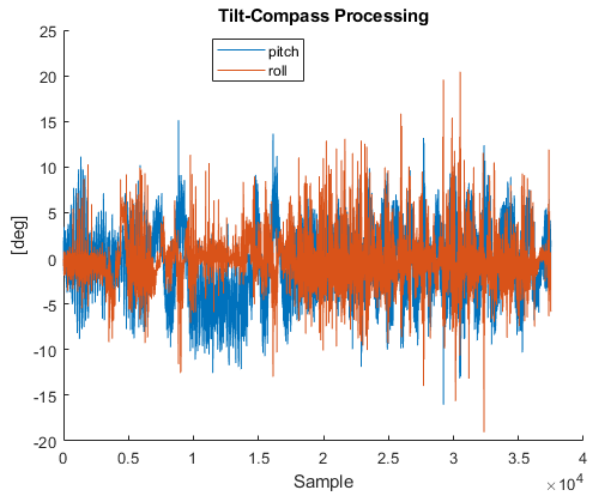

(a) E-compass algorithm

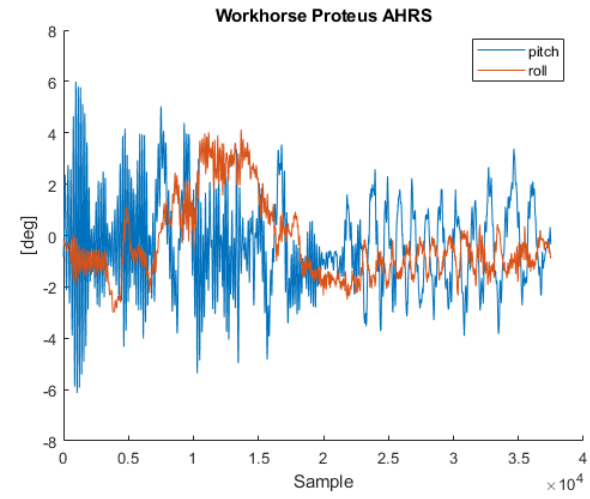

(b) Proteus AHRS

Fig. 9: Comparison of AHRS estimated attitude with e-compass estimated attitude

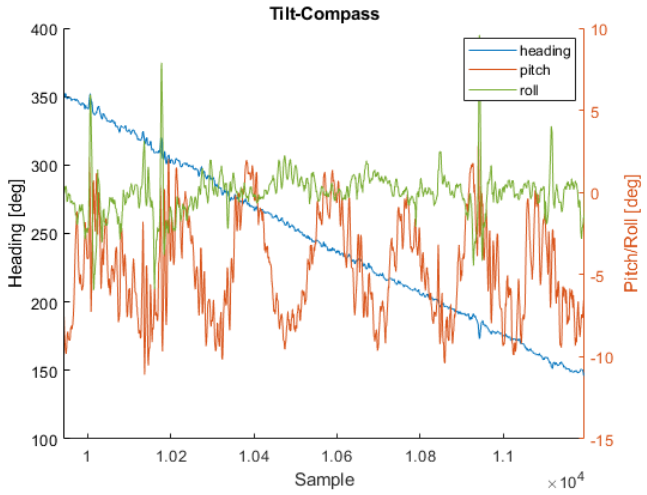

(a) E-compass algorithm

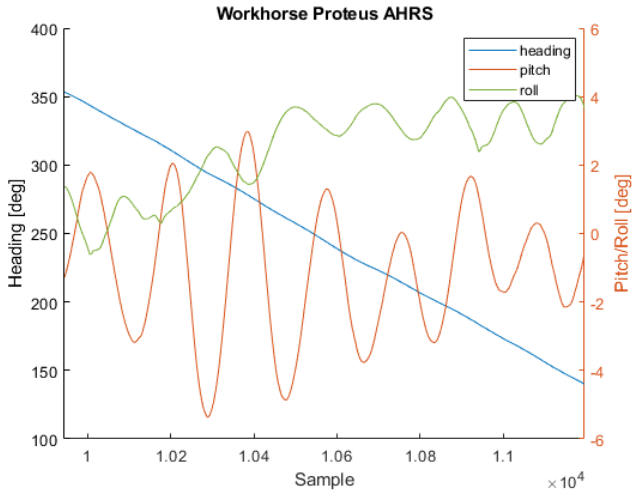

(b) Proteus AHRS

Fig. 10: Subsection comparison of AHRS estimated attitude with e-compass estimated attitude

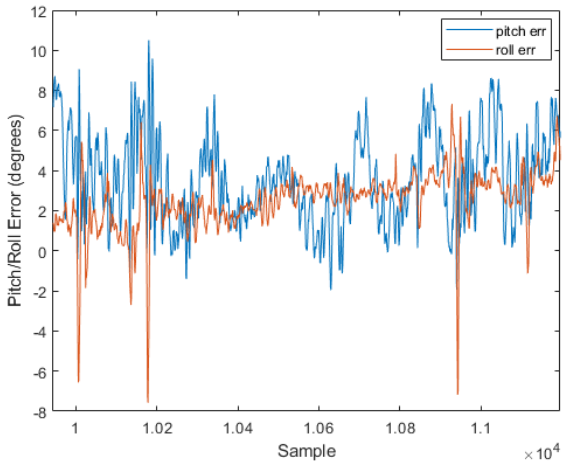

Fig. 11: Pitch and roll error of e-compass method compared to AHRS

Fig. 12: Club Moana Team

The Workhorse Proteus gyro-stabilized AHRS is not susceptible to the acceleration-induced tilt errors of the e-compass processing method. This is illustrated in Fig 10, showing the measured tilt and roll using each method while the vessel was making a steady course-correction.

The error of the e-compass method with respect to the ARHS is depicted in Fig. 11. The RMS error of the pitch and roll during this subsection was 4.2° and 2.9°, respectively.

VI. Conclusion

There exists a large and diverse set of applications for ADCPs—each of the applications can benefit from different instrument configurations and tradeoffs. A new Doppler-sonar platform called Proteus has been developed, with the objective to expand the existing ADCP tradespace to suit the wide-range of ADCP applications. A new Workhorse Proteus line of ADCPs, built on the Proteus platform was presented and an extensive set of tests were performed, including water profiling, bottom track, vessel-mounted survey, vertical beam profiling/ranging, variable transmit power, and AHRS. The test results agreed well with performance predictions and validated the new functionality of the Workhorse Proteus ADCP.

Only the 300 kHz version of the Workhorse Proteus ADCP was tested. Testing and validation of the performance of the 600 kHz and 1200 kHz versions is identified as future work.

Acknowledgment

Teledyne RD Instruments wants to thank the team from Club Moana of Cagnes Sur Mer for the focus on safety and your operational efficiency when deploying the Workhorse Proteus ADCP.

REFERENCES

[1] W. Woodward and G. Appell, "Current velocity measurements using acoustic doppler backscatter: A review," *IEEE Journal of Oceanic Engineering*, vol. 11, pp. 3–6, 1986, review¡br/¿reference.

[2] W. Wiseman, R. C. Jr., and D. Pritchard, "A three dimensional current meter for estuarine applications," *J. Marine Res.*, vol. 30, p. 1, 1972.

[3] R. Pinkel and J. A. Smith, "Repeat sequence coding for improved precision of doppler sonar and sodar," *J. Atm. and Oceanic Tech*, vol. 9, pp. 149–163, 1992.

[4] L. Regier, "Factors limiting the performance of shipboard doppler acoustic current meters," 1982, pp. 117–121.

[5] ——, "Mesoscale current fields observed with a shipboard profiling acoustic current meter," *Journal of Physical Oceanography*, vol. 12, pp. 880–886, 1982.

[6] B. H. Brumley, R. G. Cabrera, K. L. Deines, and E. A. Terray, "Performance of a broad-band acoustic doppler current profiler," *IEEE J. Ocean. Eng.*, vol. 16, pp. 402–407, 1991, broad band¡br/¿algorithm.

[7] X. Yu and L. Gordon, "38 khz broadband phased array acoustic doppler current profiler," *Proceedings of the IEEE Fifth Working Conference on Current Measurement*, pp. 53–57, 1995, phased array.

[8] J. W. Mullison, "Field verification of the pinnacle adcp," 2019, pp. 1–7.

[9] M. Jerald and P. Wanis, "2019 ieee/oes twelfth current, waves and turbulence measurement (cwtm) : 10-13 march 2019." IEEE, 2019, pp. 1–7.

[10] G. F. Appell, J. L. Chapin, and N. Trenaman, "Tests of two prototype workhorse adcps," 1995, pp. 1367–1371.

[11] A. Lohrmann and S. Nylund, "A new long range current profiler," 2013, pp. 1–7.

[12] D. W. Velasco, D. W. Wilson, S. Nylund, and R. Heitsenrether, "Enhancing the accuracy of current profiles from surface buoy- mounted systems," 2018, pp. 1–6.

[13] D. W. Velasco and S. Nylund, "Performance improvement of adcps on surface buoys," 2019, pp. 1–6.

[14] J. Y. Taudien and S. G. Bilén, "Quantifying long-term accuracy of sonar doppler velocity logs," *IEEE J. Ocean. Eng.*, vol. 43, pp. 764–776, 2018.

[15] M. A. Pinto and L. Verrier, "Interferometric doppler velocity sonar for low bias long range estimation of speed over seabed," *IEEE Journal of Oceanic Engineering*, vol. 47, pp. 767–779, 2022.

[16] J. Y. Taudien, G. Rivalan, and S. G. Bilén, "Field validation of long-term accuracy model with phased array dvls," 2017, pp. 1–6.

[17] R. J. Urick, *Principles of Underwater Sound*, 3rd ed. Peninsula Publishing, 1983.